

In-situ atomic force microscopy observation revealing gel-like plasticity on a metallic glass surface

Y. M. Lu, J. F. Zeng, J. C. Huang, S. Y. Kuan, T. G. Nieh, W. H. Wang, M. X. Pan, C. T. Liu, and Y. Yang

Citation: *Journal of Applied Physics* **121**, 095304 (2017); doi: 10.1063/1.4977856

View online: <http://dx.doi.org/10.1063/1.4977856>

View Table of Contents: <http://aip.scitation.org/toc/jap/121/9>

Published by the *American Institute of Physics*



Small Conferences. BIG Ideas.

Applied Physics
Reviews

SAVE THE DATE!
3D Bioprinting: Physical and Chemical Processes
May 2–3, 2017 • Winston Salem, NC, USA

The background of the banner features a blue-toned image of a human hand with a red, glowing, branching structure resembling a biological or chemical process overlaid on it.

In-situ atomic force microscopy observation revealing gel-like plasticity on a metallic glass surface

Y. M. Lu,^{1,2,a)} J. F. Zeng,^{1,a)} J. C. Huang,^{3,b)} S. Y. Kuan,³ T. G. Nieh,⁴ W. H. Wang,² M. X. Pan,^{2,b)} C. T. Liu,¹ and Y. Yang^{1,b)}

¹Centre for Advanced Structural Materials, Department of Mechanical and Biomedical Engineering, City University of Hong Kong, Kowloon Tong, Kowloon, Hong Kong, People's Republic of China

²Institute of Physics, Chinese Academy of Sciences, Beijing 100190, People's Republic of China

³Department of Materials and Optoelectronic Science, National Sun Yat-Sen University, Kaohsiung 80424, Taiwan

⁴Department of Materials Science and Engineering, The University of Tennessee, Knoxville, Tennessee 37996-2200, USA

(Received 19 January 2017; accepted 18 February 2017; published online 2 March 2017)

It has been decade-long and enduring efforts to decipher the structural mechanism of plasticity in metallic glasses; however, it still remains a challenge to directly reveal the structural change, if any, that precedes; and dominant plastics flow in them. Here, by using the dynamic atomic force microscope as an “imaging” as well as a “forcing” tool, we unfold a real-time sequence of structural evolution occurring on the surface of an Au-Si thin film metallic glass. In sharp contrast to the common notion that plasticity comes along with mechanical softening in bulk metallic glasses, our experimental results directly reveal three types of nano-sized surface regions, which undergo plasticity but exhibit different characters of structural evolution following the local plasticity events, including stochastic structural rearrangement, unusual local relaxation and rejuvenation. As such, yielding on the metallic-glass surface manifests as a dynamic equilibrium between local relaxation and rejuvenation as opposed to shear instability in bulk metallic-glasses. Our finding demonstrates that plasticity on the metallic glass surface of Au-Si metallic glass bears much resemblance to that of the colloidal gels, of which nonlinear rheology rather than shear instability governs the constitutive behavior of plasticity. *Published by AIP Publishing.* [<http://dx.doi.org/10.1063/1.4977856>]

I. INTRODUCTION

Extremely localized structural rearrangements under stress have long been deemed as playing a fundamental role in the mechanism of plasticity in different types of glasses, such as colloidal glass,^{1,2} oxide glass,³ polymeric glass⁴ and metallic glass (MG).^{5–9} According to the theories,¹⁰ these local sites, often being termed as loose-packing regions^{4,11,12} can be detected only in the transient when taking place at the molecular^{1,13} or atomic-scale.³ However, for MGs, the local structural rearrangements are expected to be very rapid in their mechanical response, spanning only a few nanometers at the most,^{12,14–19} therefore, it is difficult to probe and observe them directly in an *in-situ* manner. Despite that, it is generally perceived that the activation of these local sites would lead to shear softening, thereby strain localization or shear banding at the onset of yielding at a low temperature.^{6,20–22} Furthermore, the formation of shear bands in bulk metallic-glasses (BMGs) severely disrupts the amorphous structure, hence smears out the original microstructural feature prior to the yielding processes.^{23,24}

To understand the micromechanical mechanism of plasticity in MGs, Argon and co-workers employed the bubble raft experiments²⁵ in the late 1970s to mimic the inelastic

atomistic process before macroscopic yielding sets in and lead to the proposal of shear transformation zone (STZ).

In principle, each STZ was regarded by Argon *et al.* as a local plastic event that encompasses tens of loosely packed atoms, which is responsible for shear softening and subsequently triggers shear banding for yielding at low temperatures.⁶ Since then, extensive research efforts have been stimulated in the community of materials science and condensed matter physics. A variety of theoretical models, such as the different variants of the original STZ model^{7,16,18,26,27} and those based on the random first-order transition (RFOT) theory^{28,29} were developed. Many atomistic simulations were also carried out^{9,30–34} assisted with the experimental observations in colloidal glasses,^{1,13} in order to gain insights of the structural origin of plasticity in MGs. However, it is still puzzling to us what constitute the local sites that would accommodate the local structural rearrangements. The issue remains open as to whether these local plasticity events would inevitably cause local dilation and thus shear softening, as proposed in the early STZ theory,^{7,16,18,26} or they could also lead to local densification and thus hardening, at least under a certain circumstance, as can be perceived according to the recent experimental results.^{35–37} In this work, rather than investigating the local plasticity inside a BMG, we intend to elucidate the micromechanical mechanism of plasticity on a MG surface with the state-of-art dynamic atomic force microscopy (DAFM) technique.^{38–40} Different from the previous works^{11,41–43} in which DAFM

^{a)}Y. M. Lu and J. F. Zeng contributed equally to this work.

^{b)}Authors to whom correspondence should be addressed. Electronic addresses: jacobc@mail.nsysu.edu.tw; panmx@aphy.iphy.ac.cn; and yonyang@cityu.edu.hk

was used primarily for structural imaging, here we show that DAFM could be adopted as an imaging and forcing tool. As a result, we are capable of directly probing the local regions on a MG surface, trigger local plasticity events, and observe the subsequent structural evolution in an *in-situ* manner.

II. EXPERIMENTAL

In our DAFM study, a thin film metallic glass (TFMG) with the composition of $\text{Au}_{70}\text{Si}_{30}$ (in atomic percentage) was obtained via sputtering and its structural amorphousness was confirmed by X-ray diffraction (XRD) (Fig. 1(d)) and transmission electron microscopy (TEM) (Fig. 1(e)). The reason why we use thin film instead of bulk is that the DAFM is sensitive to surface roughness. Compared with the smooth thin film, fine polishing is required for bulk samples, which will damage the as-cast surface state and induce surface defects and stress. Following the DAFM method in Refs. 11 and 44, an ultra-sharp DAFM tip with a radius ~ 1 nm was used in our study. The tip was vibrating initially in air with a pre-defined amplitude A_0 and frequency ω , as illustrated in Fig. 1(a). Subsequently, it was driven to engage with a sample surface in an intermittent manner with an instantaneous amplitude $A_{sp} \sin(\omega t + \varphi)$, in which A_{sp} is the set-point amplitude and φ is the phase shift.^{38,39} From the phase shift values recorded, a phase image can be obtained point by point together with a height image.³⁸⁻⁴⁰ According to the prior works,^{11,41-44} the tip-sample contact is viscoelastic in nature, which causes energy dissipation and can be used to access the local dynamic heterogeneity in MGs. For example, Figs. 1(b) and

1(c) show the height and phase image obtained simultaneously from an $\text{Au}_{70}\text{Si}_{30}$ thin film MG, from which one can easily identify the local heterogeneities that are difficult to reveal by conventional static means, such as transmission electron microscopy. In theory, the local energy dissipation (E_{dis}) is related to the phase shift and other control/mechanical parameters of the DAFM tip via the relation $E_{dis} = \pi k A_{sp} A_0 \times (\sin(\pi/2 - \varphi) - A_{sp}/A_0)/Q$, in which k and Q denote the spring constant and quality factor of the probe, respectively.^{11,39-43} According to Ref. 45, the mean total force (F_a) exerted by the DAFM tip can be expressed as $F_a = k \times (A_0^2 - A_{sp}^2)/(2A_{sp} \times Q)$. By tuning the ratio of A_{sp}/A_0 at the same set values of A_0 , k , and Q , we can systematically change the mean force F_a and thus trigger the local structural evolution at different levels. In this study, DAFM experiments were performed at A_{sp}/A_0 ($A_0 \sim 21$ nm) ratios of 0.13, 0.25, 0.5, and 0.75, under which the tip-sample interaction remains repulsive, and the phase shift values are all positive. Correspondingly, the mean force exerted by the ultra-sharp tip ranges from 3.49 to 10.53 nN.

III. RESULTS AND DISCUSSION

To obtain the time sequence of phase imaging on the MG surface, our DAFM scanning was performed over the same surface area for a number of times at the same F_a . Following the method described in Ref. 11, we are able to remove the possible height effect out of phase imaging. Figures 2(a)–2(c) present the mapping of the local energy dissipation obtained from the $\text{Au}_{70}\text{Si}_{30}$ surface with $F_a = 3.49$ nN at different

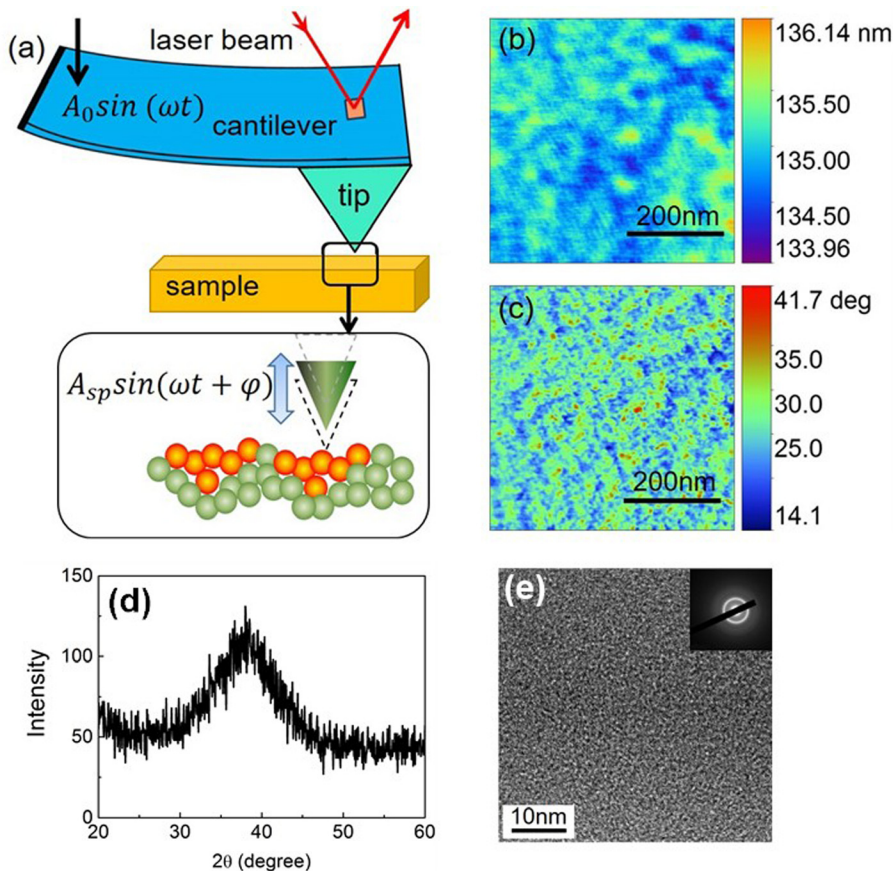


FIG. 1. (a) Schematic operating principle of the DAFM, (b) height and (c) phase images simultaneously obtained from the $\text{Au}_{70}\text{Si}_{30}$ TFMG in DAFM. (d) and (e) Show the XRD and TEM results of the $\text{Au}_{70}\text{Si}_{30}$ TFMG.

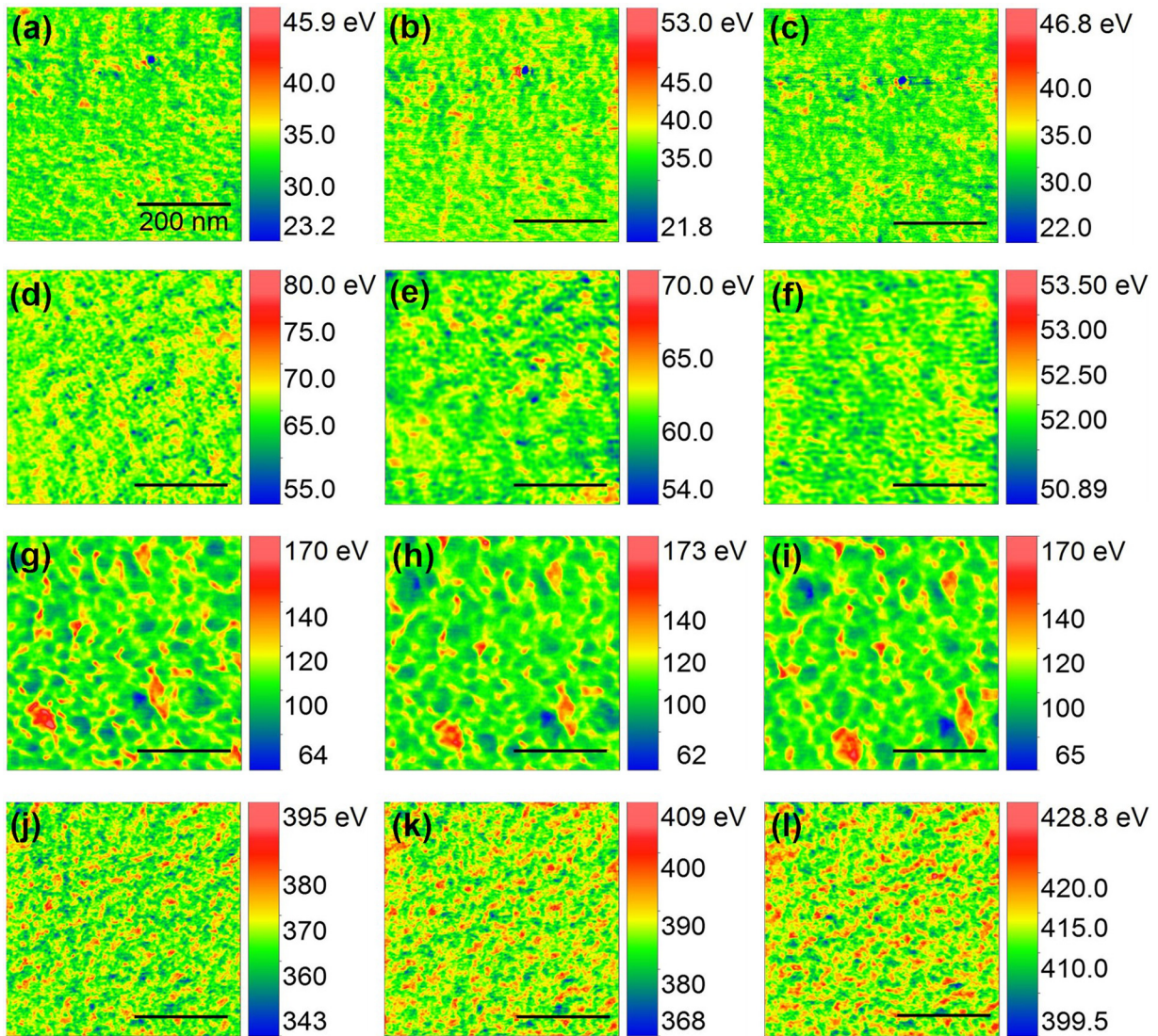


FIG. 2. Energy dissipation images of Au₇₀Si₃₀ TFMG obtained at the applied forces of (a)–(c) 3.49 nN, (d)–(f) 4.21 nN, (g)–(i) 6.75 nN, and (j)–(l) 10.53 nN, respectively. At each force, the scan numbers are 1st, 5th, and 9th. The unit of energy dissipation is the electron volt (eV).

sequences of scans. Similar to that obtained from the Zr-based TFMG,^{11,41,42} nano-scale heterogeneities were also observed on the present Au-based TFMG. There seems no significant structural evolution under this low level force ($F_a = 3.49$ nN), and the energy dissipation maps look essentially similar regardless of the number of scans (Figs. 2(a)–2(c)). However, when F_a is increased to 4.21 nN, the TFMG surface exhibits a trend of decreasing energy dissipation with the number of scans, as indicated in Figs. 2(d)–2(f). Very interestingly, such a trend of declining energy dissipation turns into a stable energy dissipation at the higher force $F_a = 6.75$ nN (Figs. 2(g)–2(i)), suggestive of a steady state. With further increasing in the mean force to $F_a = 10.53$ nN, the TFMG surface exhibits an inverse trend, namely, the energy dissipation increases with the number of scans (Figs. 2(j)–2(l)). Figures 3(a)–3(d) show the distributions of energy dissipation extracted at different number of scans at different mean forces, which describe quantitatively the results of energy dissipation images and agree very well with our direct DAFM observations (Figs. 2(a)–2(l)). Such an energy dissipation behavior on the Au-based TFMG surface is very intriguing,

which might be categorized into four types according to the order of appearance with the increasing mean total force F_a , specifically, stochastic dissipation (Fig. 3(a)), declining dissipation (Fig. 3(b)), steady-state dissipation (Fig. 3(c)) and rising dissipation (Fig. 3(d)).

To further understand the micromechanical behavior of the Au-based TFMG in our DAFM experiments, we calculated the mean elastic force F_e underneath the DAFM tip,³⁸ which can be expressed as $F_e = kA_0 \cos(\pi/2 - \Delta\phi)/(2Q)$. In general, one may take the mean total force (F_a) as the summation of the mean elastic force F_e and the mean inelastic force F_v . In such a case, the variation of the elastic force F_e with the number of scans provides us another metric to infer the underlying structural evolution on the TFMG surface. Figures 4(a)–4(d) display the variation of F_e with the number of scans at different forces. For comparison, all the mean elastic forces are normalized by the mean elastic force $F_{e\text{-ini}}$ calculated from the first scan. As a result, we can see that the mean elastic force is kept, approximately, at a constant value for the stochastic dissipation at the force of 3.49 nN (Fig. 4(a)) and the steady-state dissipation at the

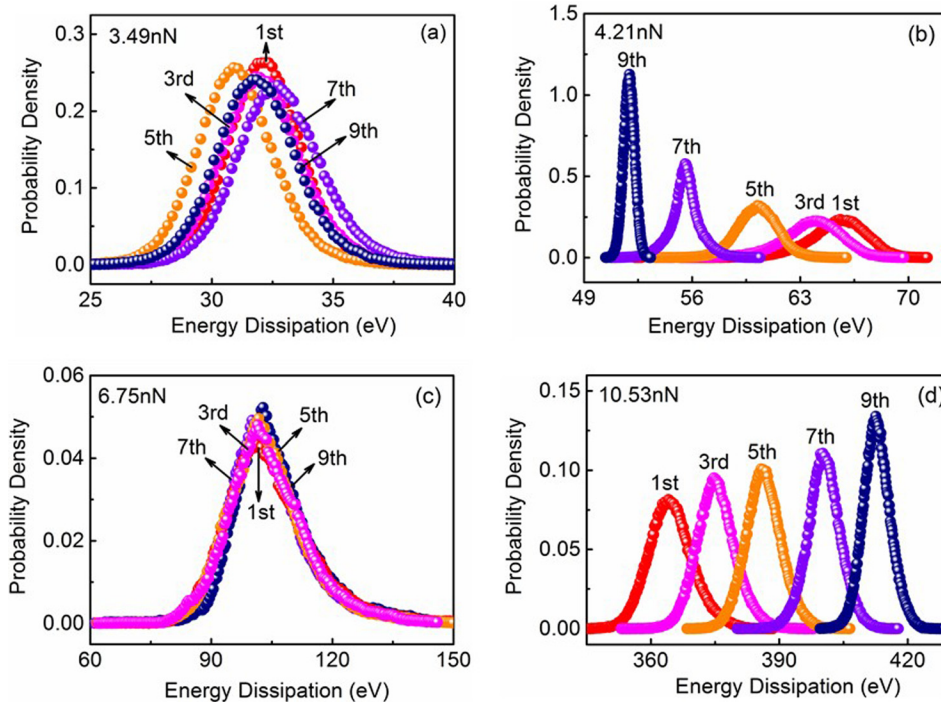


FIG. 3. Energy dissipation spectra of Au₇₀Si₃₀ TFMG obtained at the applied forces of (a) 3.49 nN, (b) 4.21 nN, (c) 6.75 nN, and (d) 10.53 nN, respectively.

force of 6.75 nN (Fig. 4(c)). In contrast, the mean elastic force increases as the energy dissipation declines at the force of 4.21 nN (Fig. 4(b)) or decreases as the energy dissipation rises at the force of 10.53 nN (Fig. 4(d)). This correlation suggests that it would be more difficult for the TFMG to dissipate energies if it became more locally elastic. This is reasonable since the viscoelastic energy dissipation in MGs stems from the presence of defect-like regions caged by their elastic surroundings.^{11,42,43} Therefore, any structural change in favor of the enhanced elastic matrix at the expense of the local defect-like regions would lead to the reduction of the local energy dissipation, and vice versa.

Next, we would like to get into a more local view of the energy dissipation on the TFMG surface. For this purpose, each energy dissipation map is divided into a square array, as shown in Fig. 5(a). For the present work, the unit size is selected to be 10 nm since it roughly corresponds to the

correlation length of the energy dissipation images (see Fig. S1, [supplementary material](#)). According to our prior work,⁴⁴ the dissipation correlation length measures the average size of the tip-sample interaction volume, which could also be viewed as the characteristic length of the spatial heterogeneity.⁴³ Interestingly, we discovered three typical dissipation behaviors by tracking each individual unit at the mean total force $F_a = 3.49$ nN. Figure 5(b) displays the dissipation behavior of type I, which exhibits a stochastic energy fluctuation and comprises the majority ($\sim 70\%$) of the TFMG surface being studied. By comparison, Fig. 5(c) shows the dissipation behavior of type II, which corresponds to an overall small but notable increase in the energy dissipation with the number of scans. In a statistic sense, type II behavior tends to appear in regions of least energy dissipation, as shown in Fig. 5(a). The dissipation behavior of type III is shown in Fig. 5(d), in which the energy dissipation initially declines and then reaches a steady state value. Meanwhile, type III is frequently found near the “boundary” regions between those showing the most and least energy dissipations (Fig. 5(a)). Similar results were also found in other regions scanned at the same total force, as shown in Fig. S2 ([supplementary material](#)). The same technique was also applied to obtain the energy dissipation maps at higher total forces, and they are shown in Fig. S3 ([supplementary material](#)). In contrast to the case of $F_a = 3.49$ nN, such a diversity of local relaxation behavior appears to be absent for those cases and only one type of relaxation unit, which conforms to the overall relaxation behavior of the energy dissipation map, could be found.

The local energy dissipation generated in DAFM is usually associated with the local structural or dynamic heterogeneity in amorphous materials, such as soft glassy materials (SGMs).^{46–48} Recently, a similar connection was also suggested for MGs by different groups.^{11,41,43,49} According to the prior works,^{11,41,43,49} the low dissipation region (LDR) is

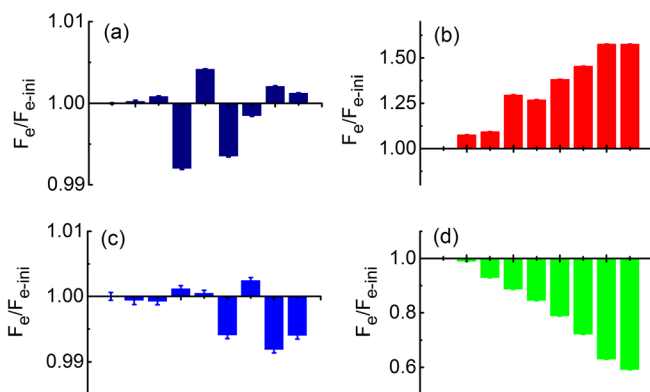


FIG. 4. The variation of elastic force (F_e) with the number of scans at the applied forces of (a) 3.49 nN, (b) 4.21 nN, (c) 6.75 nN, and (d) 10.53 nN, respectively. All the force data are normalized by the value of the respective elastic force obtained in the first scan.

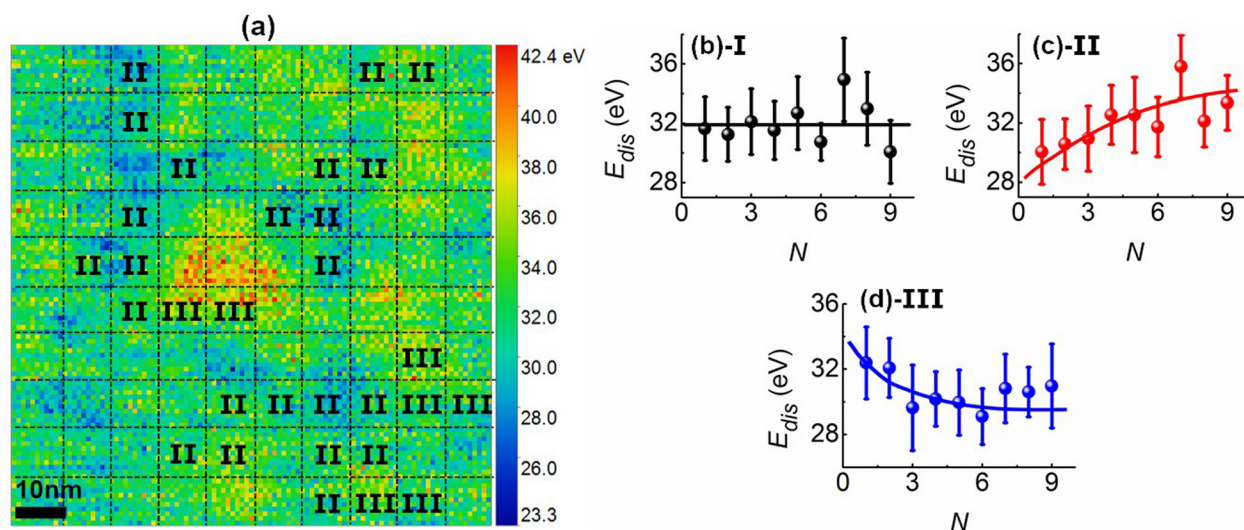


FIG. 5. (a) Distribution of the nano-sized regions on $\text{Au}_{70}\text{Si}_{30}$ TFMG surface at the mean force of 3.49 nN with unmarked units for type I and marked units for type II and type III. Type I, II, and III represent the energy dissipation behavior of (b) stochastic change, (c) continuous increase and (d) decrease with scan numbers, respectively. The solid lines in (b)–(d) are drawn for eye guides.

associated with the dense-pack structure, which tends to be more elastic and less energy dissipative, whereas the high dissipation region (HDR) with the loose-pack structure tends to be more viscoelastic and more energy dissipative. This structural connection was theoretically validated through the mean-field model developed by Liu and Yang⁴⁹ and is also in agreement with the recent experimental findings in mechanical relaxation of MGs.⁴³ Based on this understanding, the shifting of the energy distribution with the number of scans, such as those shown in Figs. 3(a)–3(d), is indicative of the change of atomic-packing density on the TFMG surface with the repeated AFM scanning. To be more specific, the declining energy dissipation can be interpreted as a manifestation of stress-induced densification on the TFMG surface (Fig. 3(b)) while the rising energy dissipation is associated with stress-induced dilation (Fig. 3(d)). From a nanoscale perspective, the densification (dilation) results from the stress-induced evolution of the nano-sized regions, such as HDRs. As shown in Fig. S4 (supplementary material), when the energy dissipation declines, the shrinkage of the HDRs was observed; by contrast, proliferation of the HDRs with very limited growth was observed when the average energy dissipation rises. As such, from the thermodynamic point of view, the four types of energy dissipation behavior, shown in Figs. 3(a)–3(d), simply suggest that the TFMG underwent a four-step evolution process as the mean total force increased—starting from a stochastic process featured by local structural rearrangements (Fig. 3(a)) to a more deterministic process of structural relaxation (densification) (Fig. 3(b)) until reaching an apparent dynamic equilibrium (Fig. 3(c)), and finally a deterministic process of structural rejuvenation (dilation) (Fig. 3(d)). This is drastically different from the classic picture that local plastic event mainly leads to dilation or rejuvenation, till finally triggering a shear instability in BMGs at low temperatures.^{6,20–22} Notably, Packard *et al.*³⁵ reported a similar phenomenon of stress-induced relaxation or hardening under spherical nano-indentation, which is consistent with our current *in-situ* DAFM observations.

Although our present findings of the surface plasticity may appear unusual to MGs, however, similar phenomena were frequently observed in soft glassy materials (SGMs), such as colloidal suspensions,^{50–52} emulsions⁵³ and granular matters.⁵³ For most SGMs, plasticity is governed by a nonlinear rheology rather than shear instability. Because of the relatively low packing density, the amorphous structure of these materials tends to relax under a small mechanical perturbation, leading to an increase in the overall viscosity and eventually the arrest of any incipient flow. By contrast, their amorphous structure tends to rejuvenate under a large mechanical perturbation, leading to a decrease in the overall viscosity and the acceleration of the incipient flow. Consequently, yielding in most SGMs manifests as a dynamic equilibrium between stress-induced relaxation and rejuvenation, which is very similar to what we currently observe on the surface of the Au-based TFMG. In addition, for MGs, previous experiments⁵⁴ and theories¹⁰ already demonstrated that dynamics on glass surface is much faster than in the bulk. In comparison, it is reasonable to assume that the surface of our Au-based TFMG is liquid-like, which behaves in a similar fashion as those soft glassy materials. Based on our DAFM results, we estimate the viscosity of the Au-based TFMG to be 10^5 – 10^6 Pa s on the surface, which is much lower than the bulk viscosity ($\sim 10^{12}$ Pa s) at the glass transition temperature (see the supplementary material for viscosity calculation). To further verify that the gel-like surface plasticity was indeed from a low-density amorphous structure, we annealed our Au-based TFMG to crystallization and then performed identical experiments (see Fig. S5, supplementary material), no shifting of the energy distribution was observed after thermal annealing. In fact, the liquid-like features near surface, which contribute to the gel-like plasticity observed in our work, should be a general phenomenon of MGs. Both theory and experimental results have shown that the liquid-like features are independent of sample dimensions and could also be found in bulk samples.

Based on the above analyses, now we can estimate the surface yielding strength of our TFMG. For this purpose, we

take $F_a = 6.75$ nN as the critical force that corresponds to the dynamic equilibrium as indicated in Fig. 3(c). Furthermore, we assume a full contact between the AFM tip and the surface with the contact size ~ 1 nm. The surface yielding stress is subsequently estimated to be ~ 0.7 GPa, which is about one half of the yielding stress ~ 1.3 GPa of the bulk Au₇₀Si₃₀ BMG (see the [supplementary material](#) for the calculation of yielding stress). Since the yielding stress τ_y in MGs is correlated with their glass transition point^{55,56} T_g , i.e., $\tau_y \sim (T_g - T)$, where T is the ambient temperature, the estimated yield stress (~ 0.7 GPa) then implies that the glass transition point at the TFMG surface should be significantly lower than that in the bulk. Since the typical T_g for Au-based BMGs is around 400 K,⁵⁷ we can then estimate that T_g on the surface of our Au-based TFMG is ~ 353 K, very close to the room temperature. For polymeric glass films, people reported the reduction of the glass transition point when the film thickness decreases,^{58–60} which also agrees with our current finding. However, to our best knowledge, the size-dependent glass transition behavior has not been directly observed yet for MGs. As a final note, it is worth pointing out that, depending on the chemical composition, some MGs may possess a stable surface, as discussed in Refs. 61–63, which is difficult to observe the gel-like plasticity on the surface.

IV. CONCLUSION

In summary, we report the surface plasticity behavior of the Au-based TFMG by directly probing stress-induced structural evolution. Through *in-situ* DAFM observations, we observed the nano-sized regions which exhibit unusual characteristics of structural evolution immediately after the local plasticity. Unlike BMGs, whose plasticity is governed by local softening and shear instability, the Au-based TFMG surface exhibits gel-like plasticity similar to those occurring in soft glassy materials, such as colloidal gels and suspensions. These interesting findings suggest a nonuniform glassy structure near the surface of the Au-based TFMG, which can be further explored for important applications, such as nano-scale lubrication and self-healing.

SUPPLEMENTARY MATERIAL

See [supplementary material](#) for the calculation of viscosity and yielding stress.

ACKNOWLEDGMENTS

Y.Y. is grateful for the financial support provided by the Research Grant Council (RGC), the Hong Kong government through the General Research Fund (GRF) with the Grant No. 11214914, the NSF of China with the Grant No. 51271195 and the MOST 973 Program (No. 2015CB856800).

¹P. Schall, D. A. Weitz, and F. Spaepen, *Science* **318**, 1895 (2007).

²V. Chikkadi, G. Wegdam, D. Bonn, B. Nienhuis, and P. Schall, *Phys. Rev. Lett.* **107**, 198303 (2011).

³P. Y. Huang, S. Kurasch, J. S. Alden, A. Shekhawat, A. A. Alemi, P. L. McEuen, J. P. Sethna, U. Kaiser, and D. A. Muller, *Science* **342**, 224 (2013).

⁴J. Y. Cavaille, J. Perez, and G. P. Johari, *Phys. Rev. B* **39**, 2411 (1989).

⁵F. Spaepen, *Acta Metall.* **25**, 407 (1977).

⁶A. Argon, *Acta Metall.* **27**, 47 (1979).

⁷M. L. Falk and J. S. Langer, *Phys. Rev. E* **57**, 7192 (1998).

⁸P. Luo, Y. Z. Li, H. Y. Bai, P. Wen, and W. H. Wang, *Phys. Rev. Lett.* **116**, 175901 (2016).

⁹D. Srolovitz, V. Vitek, and T. Egami, *Acta Metall.* **31**, 335 (1983).

¹⁰J. D. Stevenson and P. G. Wolynes, *J. Chem. Phys.* **129**, 234514 (2008).

¹¹Y. Yang, J. F. Zeng, A. Volland, J. J. Blandin, S. Gravier, and C. T. Liu, *Acta Mater.* **60**, 5260 (2012).

¹²J. Ye, J. Lu, C. Liu, Q. Wang, and Y. Yang, *Nat. Mater.* **9**, 619 (2010).

¹³X. Yang, R. Liu, M. Yang, W.-H. Wang, and K. Chen, *Phys. Rev. Lett.* **116**, 238003 (2016).

¹⁴D. Pan, A. Inoue, T. Sakurai, and M. Chen, *Proc. Natl. Acad. Sci.* **105**, 14769 (2008).

¹⁵L. Huo, J. Zeng, W. Wang, C. T. Liu, and Y. Yang, *Acta Mater.* **61**, 4329 (2013).

¹⁶Y. Fan, T. Iwashita, and T. Egami, *Nat. Commun.* **5**, 5083 (2014).

¹⁷S. Mayr, *Phys. Rev. Lett.* **97**, 195501 (2006).

¹⁸W. L. Johnson and K. Samwer, *Phys. Rev. Lett.* **95**, 195501 (2005).

¹⁹H. B. Yu, W. H. Wang, H. Y. Bai, Y. Wu, and M. W. Chen, *Phys. Rev. B* **81**, 220201 (2010).

²⁰H. Bei, S. Xie, and E. P. George, *Phys. Rev. Lett.* **96**, 105503 (2006).

²¹J. Pan, Q. Chen, L. Liu, and Y. Li, *Acta Mater.* **59**, 5146 (2011).

²²F. Spaepen, *Nat. Mater.* **5**, 7 (2006).

²³W. H. Wang, Y. Yang, T. G. Nieh, and C. T. Liu, *Intermetallics* **67**, 81 (2015).

²⁴R. Dasgupta, H. G. E. Hentschel, and I. Procaccia, *Phys. Rev. Lett.* **109**, 255502 (2012).

²⁵A. Argon and H. Kuo, *Mater. Sci. Eng.* **39**, 101 (1979).

²⁶J. S. Langer, *Phys. Rev. E* **70**, 041502 (2004).

²⁷T. Egami, *Prog. Mater. Sci.* **56**, 637 (2011).

²⁸T. R. Kirkpatrick, D. Thirumalai, and P. G. Wolynes, *Phys. Rev. A* **40**, 1045 (1989).

²⁹T. R. Kirkpatrick and P. G. Wolynes, *Phys. Rev. B* **36**, 8552 (1987).

³⁰P. Cao, X. Lin, and H. S. Park, *Phys. Rev. E* **90**, 012311 (2014).

³¹C. E. Maloney and A. Lemaître, *Phys. Rev. E* **74**, 016118 (2006).

³²Y. Cheng, A. J. Cao, H. Sheng, and E. Ma, *Acta Mater.* **56**, 5263 (2008).

³³S. Kobayashi, K. Maeda, and S. Takeuchi, *Acta Metall.* **28**, 1641 (1980).

³⁴J. Ding, S. Patinet, M. L. Falk, Y. Cheng, and E. Ma, *Proc. Natl. Acad. Sci.* **111**, 14052 (2014).

³⁵C. Packard, L. Witmer, and C. Schuh, *Appl. Phys. Lett.* **92**, 171911 (2008).

³⁶Z. T. Wang, J. Pan, Y. Li, and C. A. Schuh, *Phys. Rev. Lett.* **111**, 135504 (2013).

³⁷Y. Yang, X. Fu, S. Wang, Z. Liu, Y. Ye, B. Sun, and C. Liu, *Sci. Rep.* **4**, 6699 (2014).

³⁸Á. San Paulo and R. García, *Phys. Rev. B* **64**, 193411 (2001).

³⁹M. Stark, C. Möller, D. J. Müller, and R. Guckenberger, *Biophys. J.* **80**, 3009 (2001).

⁴⁰J. P. Cleveland, B. Anczykowski, A. E. Schmid, and V. B. Elings, *Appl. Phys. Lett.* **72**, 2613 (1998).

⁴¹Y. H. Liu, D. Wang, K. Nakajima, W. Zhang, A. Hirata, T. Nishi, A. Inoue, and M. W. Chen, *Phys. Rev. Lett.* **106**, 125504 (2011).

⁴²J. F. Zeng, J. P. Chu, Y. C. Chen, A. Volland, J. J. Blandin, S. Gravier, and Y. Yang, *Intermetallics* **44**, 121 (2014).

⁴³F. Zhu, H. Nguyen, S. Song, D. P. Aji, A. Hirata, H. Wang, K. Nakajima, and M. Chen, *Nat. Commun.* **7**, 11516 (2016).

⁴⁴Y. M. Lu, J. F. Zeng, S. Wang, B. A. Sun, Q. Wang, J. Lu, S. Gravier, J. J. Blandin, W. H. Wang, M. X. Pan, C. T. Liu, and Y. Yang, *Sci. Rep.* **6**, 29357 (2016).

⁴⁵S. Morita, *Roadmap of Scanning Probe Microscopy* (Springer Science & Business Media, 2006).

⁴⁶R. Garcia, C. J. Gómez, N. F. Martínez, S. Patil, C. Dietz, and R. Magerle, *Phys. Rev. Lett.* **97**, 016103 (2006).

⁴⁷R. Garcia, R. Magerle, and R. Perez, *Nat. Mater.* **6**, 405 (2007).

⁴⁸D. Klinov and S. Magonov, *Appl. Phys. Lett.* **84**, 2697 (2004).

⁴⁹Z. Y. Liu and Y. Yang, *Intermetallics* **26**, 86 (2012).

⁵⁰B. Daniel, T. Sorin, A. Bérengère, T. Hajime, and M. Jacques, *Phys. Rev. Lett.* **89**, 015701 (2002).

⁵¹P. Coussot, Q. D. Nguyen, H. T. Huynh, and D. Bonn, *J. Rheol.* **46**, 573 (2002).

⁵²C. Philippe, Q. D. Nguyen, H. T. Huynh, and B. Daniel, *Phys. Rev. Lett.* **88**, 175501 (2002).

- ⁵³F. Da Cruz, F. Chevoir, B. Daniel, and P. Coussot, *Phys. Rev. E* **66**, 051305 (2002).
- ⁵⁴C. R. Cao, Y. M. Lu, H. Y. Bai, and W. H. Wang, *Appl. Phys. Lett.* **107**, 141606 (2015).
- ⁵⁵B. Yang, C. T. Liu, and T. G. Nieh, *Appl. Phys. Lett.* **88**, 221911 (2006).
- ⁵⁶Y. H. Liu, C. T. Liu, W. H. Wang, A. Inoue, T. Sakurai, and M. W. Chen, *Phys. Rev. Lett.* **103**, 065504 (2009).
- ⁵⁷B. Lohwongwatana, Ph.D. thesis, California Institute of Technology, 2007.
- ⁵⁸J. A. Forrest, K. Dalnoki-Veress, J. R. Stevens, and J. R. Dutcher, *Phys. Rev. Lett.* **77**, 2002 (1996).
- ⁵⁹J. A. Forrest and J. Mattsson, *Phys. Rev. E* **61**, R53 (2000).
- ⁶⁰J. L. Keddie, R. A. Jones, and R. A. Cory, *Europhys. Lett.* **27**, 59 (1994).
- ⁶¹H. B. Yu, Y. Luo, and K. Samwer, *Adv. Mater.* **25**, 5904 (2013).
- ⁶²J. Q. Wang, N. Chen, P. Liu, Z. Wang, D. V. Louzguine-Luzgin, M. W. Chen, and J. H. Perepezko, *Acta Mater.* **79**, 30 (2014).
- ⁶³S. Singh, M. D. Ediger, and J. J. de Pablo, *Nat. Mater.* **12**, 139 (2013).